Available online at www.sciencedirect.com
ScienceDirect
Acta Materialia 59 (2011) 283–296
Acta MATERIALIA
www.elsevier.com/locate/actamat

Energy of slip transmission and nucleation at grain boundaries

Michael D. Sangid [a], Tawhid Ezaz [a], Huseyin Sehitoglu [a,*], Ian M. Robertson [b]

[a] Department of Mechanical Science and Engineering, University of Illinois at Urbana-Champaign, 1206 W. Green St., Urbana, IL 61801, USA
[b] Department of Material Science and Engineering, University of Illinois at Urbana-Champaign, 1304 W. Green St., Urbana, IL 61801, USA

Received 25 March 2010; received in revised form 14 September 2010; accepted 16 September 2010
Available online 19 October 2010

Abstract

Grain boundaries (GBs) provide a strengthening mechanism in engineering materials by impeding dislocation motion. In a polycrystalline material, there is a wide distribution of GB types with characteristic slip transmission and nucleation behaviors. Slip–GB reactions are not easy to establish analytically or from experiments; furthermore, there is a strong need to quantify the energy barriers of the individual GBs. We introduce a methodology to calculate the energy barriers during slip–GB interaction, in concurrence with the generalized stacking fault energy curve for slip in a perfect face-centered cubic material. By doing so, the energy barriers are obtained at various classifications of GBs for dislocation transmission through the GB and dislocation nucleation from the GB. The character and structure of the GB plays an important role in impeding slip within the material. The coherent twin ($\Sigma3$) boundary provides the highest barrier to slip transmission. From this analysis, we show that there is a strong correlation between the energy barrier and interfacial boundary energy. GBs with lower static interfacial energy offer a stronger barrier against slip transmission and nucleation at the GB. The results of our simulations are in agreement with experimental observations as demonstrated for $\Sigma3$, $\Sigma13$ and $\Sigma19$ boundaries. The $\Sigma3$ GB represents a higher-energy barrier compared to the $\Sigma13$ and $\Sigma19$ GBs, where, for the latter case, complex stacking fault structures are present in experiments and simulations.

Keywords: Grain boundary energy; Molecular dynamics simulations (MD simulations); Coincidence site lattice (CSL); Dislocation; Slip

1. Introduction

It is well established that grain boundaries (GBs) offer a substantial strengthening mechanism within materials [1]. At the atomic level, the physics of the energy barriers produced by GBs is still an unresolved issue, including the individual strengthening benefit of various types of GBs. These energy barriers are essential to the understanding of plastic deformation and have tremendous implications, especially for failure mechanisms such as fatigue, fracture and creep. In classical treatments, GBs were proposed to impede dislocation motion resulting in pile-ups at the GB, which in turn provides a stress concentration that activates dislocation sources in neighboring grains [2,3]. In later works, the focus has been on incident dislocations reactions with GBs, which produce residual dislocations at the interface [1] and modify the energy barriers for incorporation and transmission processes. The precise magnitude of the energy barriers, as influenced by the underlying reactions and obstacles, has not been established previously and is the main focus of this work. Specifically, the relative magnitudes of energy barriers for transmission vs. nucleation are highlighted for various types of GBs.

The role that individual interfaces play on the mechanical behavior of a material is a very hard phenomenon to observe experimentally. To simplify this analysis, many experiments have been conducted on a bicrystal, which allows researchers to study deformation and incompatibilities across a single grain boundary [1,4]. The research of Livingston and Chalmers [5] created a criterion for slip across a grain boundary based on the geometry of the system. This geometrical criterion was extended by Shen, Wagoner and Clark in 1986, who noted that the resolved shear stress should be maximized [6]. In 1989, Lee, Robertson and Birnbaum

* Corresponding author. Tel.: +1 217 333 4112; fax: +1 217 244 6534.
E-mail address: huseyin@illinois.edu (H. Sehitoglu).

1359-6454/$36.00 © 2010 Acta Materialia Inc. Published by Elsevier Ltd. All rights reserved.
doi:10.1016/j.actamat.2010.09.032

(LRB) proposed the addition of a third requirement, namely that the residual dislocation in the grain boundary be minimized [7]. The aforementioned studies [5–7] are very valuable and outline strain incompatibility at the grain boundary, although they do not address the energy barriers that dislocations must overcome to penetrate the grain boundary.

In order for a dislocation to penetrate a GB, there must exist sufficient applied stress to drive the incident dislocations past the stress field of the GB [8]. The slip–GB interaction is governed by the degree to which the system can relax the local stress concentrations, which govern the possible cases as outlined by Sutton and Balluffi [9]: (i) direct transmission, (ii) direct transmission including residual dislocations in the GB, (iii) indirect transmission including residual dislocations in the GB where the incident and outgoing slip systems do not intersect, and (iv) no transmission—the dislocation is incorporated in the GB. In the last 40 years, there has been significant experimental work and analysis of the slip–twin [10–20] and slip–GB interactions [16–18,20–22]. In the majority of these cases, the incident dislocation dissociates into an outgoing dislocation transmitting through the GB and a residual dislocation within the GB. Table 1 provides a summary of experimental observations of slip–twin and slip–GB interactions, although, for the sake of brevity, a detailed review of these interactions is not discussed in the present paper as the focus of this study is on the resulting energy barriers. In Table 1, we have attempted to collect the best-known investigations on face-centered cubic (fcc) metals, where GB types have been identified. In many cases, transmission occurs with residual dislocations at the boundary (TRD) consistent with the results presented here. The energy barriers associated with each boundary type are not easy to quantify from experiments but are extremely relevant to crystal plasticity modeling, as well as predictions of slip in fatigue, creep and fracture.

The activation energy in a material represents a barrier to slip and plastic flow. This parameter is dependent on the stress, temperature and strain rate as discussed by Seeger [23,24]. To better represent this concept, the activation energy has been separated into thermal and athermal components. Conrad outlined a methodology to calculate athermal energies from experiments [25]. Meanwhile, Kocks proposed that the thermal component of the activation energy can be back-calculated by fitting a functional form of the Arrhenius law to experimental data of single or polycrystalline material [26–28]. This methodology has served the materials community well, although it does not shed light into the activation energy for individual GBs within an aggregate, as is the focus of this study; to do so, we must characterize individual grain boundary types.

By including the nature of the grain boundary, we can model GBs as rotations of lattices of type: twist, tilt or mixed. It should be expected that a certain number of the atoms in each of the lattice have coincidental locations. This is known as a coincident site lattice (CSL). As shown in Fig. 1, the CSL value is calculated by taking the ratio of the total number of atoms at the interface to those atoms that are in coincidental sites from each lattice. In each schematic, grains are differentiated by solid circle exteriors and shaded interiors with the colors designating the stacking sequence about their respective planes for a fcc material. Fig. 1a displays a coherent twin boundary also known as a $\Sigma 3$ GB, in which 3 out of 9 atoms match the spatial location and stacking sequence (similar colors). Similarly,

Table 1
Review of the experimentally observed slip–twin and slip–GB interactions, where *TRD** denotes the case of transmission including residual dislocations in the GB. Note that the CSL Σ value does not represent a full (5 degrees of freedom) description of the GB; hence the CSL Σ values reported in these studies are not unique descriptions of the GB.

CSL Σ boundary	Investigator, Material, and reference	Interaction result
$\Sigma 3$	Lim (1984): Ni [10]	Direct transmission
$\Sigma 3$	Venables (1961): Cu [11]; Saito (1970): Cu–4 wt.% Ti [12]; Mahajan and Chin (1973): Co–8 wt.%. Fe [13]; Remy (1977): Co–8 wt.% Fe [14]; Evans (1974): α-Brass [15]; Darby, Schindler and Balluffi (1978): Au [16]; Dingley and Pond (1979): Al [17]; Lim and Raj (1985): Ni [18]	*TRD**
$\Sigma 3$	Shen, Wagoner and Clark (1988): 304 Stainless Steel [19]; Lee, Robertson and Birnbaum (1990): 310 Stainless Steel [20]	Dislocation pile-up resulting in eventual transmission; *TRD**
$\Sigma 5$	Darby, Schindler and Balluffi (1978): Au [16]	*TRD**
$\Sigma 9$	Darby, Schindler and Balluffi (1978): Au [16]; Lim and Raj (1985): Ni [18]	*TRD**
$\Sigma 9$	Kurzydlowski, Varin and Zielinski (1984): austenitic stainless steel [21]	Emitted dislocation from GB
$\Sigma 11$	Lim and Raj (1985): Ni [18]	*TRD**
$\Sigma 13$	Lee, Robertson and Birnbaum (1990): 310 stainless steel [20]	Dislocation pile-up resulting in eventual transmission; *TRD**
$\Sigma 17$	Ishida, Hasegawa and Nagata (1969): Fe–0.75 wt.% Mn [22]	*TRD**
$\Sigma 19$	Lee, Robertson and Birnbaum (1990): 310 stainless steel [20]	Pile-up leading to indirect slip transmission; *TRD**
$\Sigma 27$	Lim and Raj (1985): Ni [18]	*TRD**
$\Sigma 33$	Lim and Raj (1985): Ni [18]	*TRD**
$\Sigma 41$	Dingley and Pond (1979): Al [17]; Lim and Raj (1985): Ni [18]	*TRD**
$\Sigma 57$	Lim and Raj (1985): Ni [18]	*TRD**
$\Sigma 89$	Lim and Raj (1985): Ni [18]	*TRD**

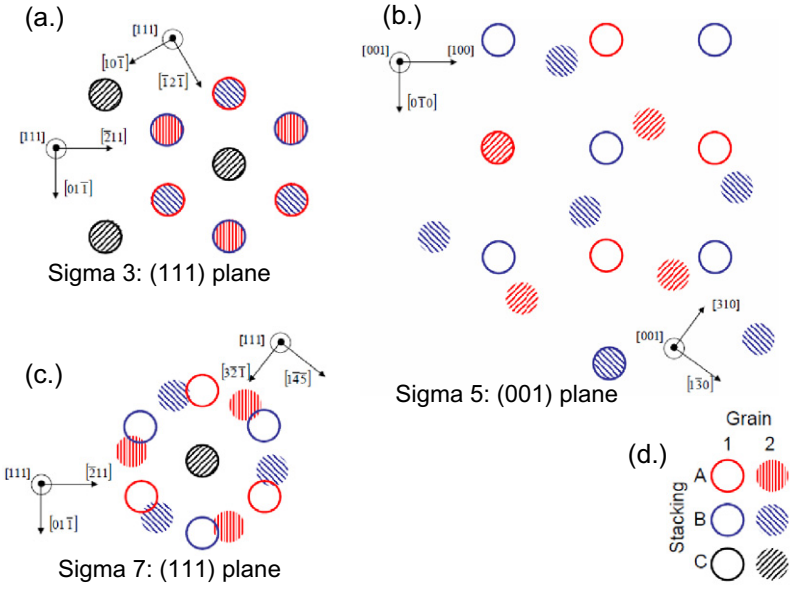

Fig. 1. Schematic of CSL GBs. (a) Σ3 GB, coherent twin boundary (3 out of 9 atoms are in coincidence). (b) Σ5 GB (2 out of 10 atoms are in coincidence). (c) Σ7 GB (1 out of 7 atoms are in coincidence). (d) In each schematic, grain 1 is represented with solid circle exteriors, grain 2 is represented with shaded interiors, and the stacking sequence is indicated by the various colors (ABC stacking (red, blue, black) for the (1 1 1) planes as shown in (a) and (c) and AB stacking (red, blue) for the (0 0 1) plane as shown in (b). When the symbols spatially align with similar colors, the atoms are in coincidental lattice positions as indicated by for (a), and for (b), and for (c).

schematics for the Σ5 (2 out of 10 atoms) and Σ7 (1 out of 7 atoms) GBs are shown in Fig. 1b and c, respectively. Further, special GBs arise as a consequence of the CSL [29]. As the importance of the CSL became more widely recognized, the mathematics of GBs were developed to handle their configuration [30].

Sutton and Vitek proposed that the GB energy be attributed to the structural units that comprise the interface [31,32]. From this work, Rittner and Seidman clearly described a technique for generating the GB energies for the structure of the GBs and the resulting dislocation structure [33]. The CSL configuration was adopted in these simulations, where the calculations represent static energies; many of the procedures used in these studies aid the current work. Building on these investigations, modeling dislocation nucleation from GBs of nanocrystalline material has provided insight at smaller length scales [34,35]. Although the stresses necessary to nucleate the dislocation from these pristine GBs were calculated correctly for ideal cases [36–39], they are much too high. The excessive value of the simulation stress is indicative of the molecular dynamics (MD). In the present work, we are concerned with the deformation in larger scales; thus we extract information from atomistic simulations for modeling bulk material on the energy magnitudes, and circumvent the use of stress as a state variable.

There are several slip–GB interaction simulations that offer a qualitative understanding of the role of GBs in strengthening the material [40–51], although these studies do not address the energy barriers of slip–GB interactions which are the focus of our study. There have been few attempts to use MD to quantify the activation energy associated with deformation, although these studies have focused on Kocks' approach for deformation of a nanocrystalline aggregate [52] or the use of the nudged elastic band method [53–55].

We produce a new methodology for the energy barriers that dislocations must overcome to penetrate GBs. These energy barriers are shown to depend on the characteristic of the individual GB. We predict the correct barriers for simple cases, as shown based on the generalized stacking fault energy (GSFE). In addition, the correct trends are predicted such as the difficulty to penetrate Σ3 boundaries (coherent twin boundaries), and the ease to penetrate a defect-free fcc lattice, consistent with experiments.

The paper discusses the simulation results in light of experimental evidence from the literature and also in situ transmission electron microscopy (TEM), which led to the LRB criteria. The results show consistency with the LRB criteria for transmission, with specific illustrations of simulations and in situ TEM comparisons for Σ13 and Σ19 GBs. We discuss all possible reactions for the slip transmission through a Σ11 GB and demonstrate that the simulation results are in agreement with the LRB criteria. The difficulty in penetrating the Σ3 GB is demonstrated experimentally and in simulations. Most importantly, we provide the energy barriers associated with nucleation and transmission of dislocations at specific GBs, which offers substantial advancement to future modeling efforts.

2. Simulation methods

To capture the physics at the GB interface, it is necessary to investigate this problem at a smaller scale. Atomic simulations were utilized in the form of a MD code called

LAMMPs [56,57] to study the effects of GB misorientation on the energy of its interface and to service our model. A system was set-up to investigate a grain with a specific (mis)orientation "sandwiched" between two similar grains, representing a specific tilt or twist GB with a corresponding CSL Σ value, as shown in Fig. 2. Grains 1 and 2 in the structure were created with a specific orientation to represent distinct CSL boundaries [58], in which the boundary plane is represented by ***n***. For tilt and twist GBs, the axis of rotation is aligned with ***c*** and ***n***, respectively.

In each structure, the fcc lattice is comprised of atoms with the Foiles–Hoyt Ni embedded atom method (EAM) potential [59]. This EAM potential for Ni was chosen to match the intrinsic, γ_{SF}-127 mJ m^{-2}, and unstable, γ_{US}-255 mJ m^{-2}, stacking fault energies of the material, which compare well with experimental values of 125–128 mJ m^{-2} and ab initio calculations of 273 mJ m^{-2} for the γ_{SF} and γ_{US} energies, respectively [60]. It is critical to obtain reasonable values of the unstable stacking fault energy as this parameter has been tied to the mechanics and nucleation of dislocations [61]. Also, the lattice constant of this EAM potential, 3.52 Å, exactly matches that of nickel. Periodic boundary conditions are enforced in all three directions to represent bulk material, and the simulation cell is of sufficient size (*L, B, W* refer to Fig. 2) to negate boundary–boundary strain field interactions or "cross-talk" of the GBs:

$$L = \alpha\sqrt{h^2 + k^2 + l^2} \geqslant 8 \text{ nm}, \tag{1}$$

$$B, W = \beta\sqrt{h^2 + k^2 + l^2} \geqslant 5 \text{ nm}, \tag{2}$$

where *h, k, l* are the Miller indices for the three orthogonal vector representations of each grain orientation and α and β are scalars to satisfy the size requirements. The system is first annealed to 800 K and then quenched to 10 K; afterwards the atoms are statically equilibrated or "relaxed" using the conjugant gradient method to obtain the energy of the system. Further, the box dimension in only the direction normal to the GB was allowed to relax in order to alleviate any GB pressure.

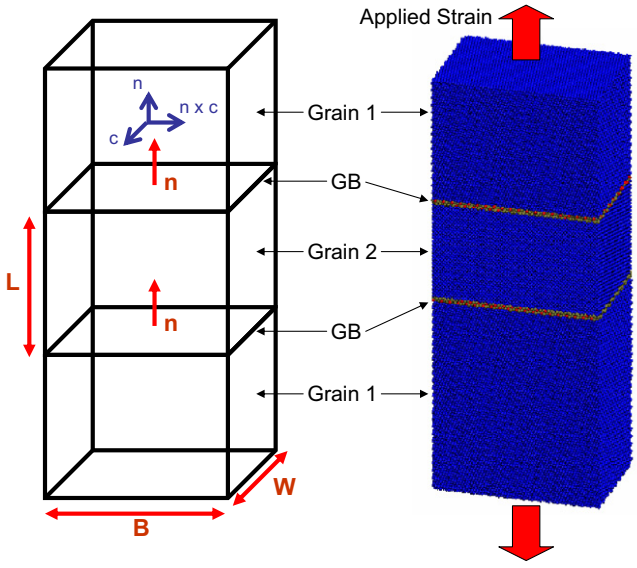

Fig. 2. Grain boundary set-up for the atomic simulation. For tilt and twist GBs, the axis of rotation is represented by **c** and **n**, respectively.

For a dislocation to interact with a GB, it is necessary to have a single controlled dislocation nucleating within the simulation and traveling towards the GB. This is accomplished by inserting a single spherical void within the simulation box below the GB, which acts as a stress concentrator to nucleate a dislocation and facilitate a slip–GB interaction. Care is taken to ensure that the strain field from the void does not interact with the strain field produced by the G; thus the void is placed sufficiently far away from the GBs. After insertion of the void, the system is statically and dynamically relaxed using an *NPT* ensemble where the number of atoms in the simulation box, *N*, the pressure in the three directions (stress free boundaries), *P*, and the system temperature, *T* (10 K), are held constant throughout the simulation.

In order to study the mechanical behavior of the GBs and measure their strengthening contribution via energy barriers to plastic flow, we must add forces and observe the kinetics of the GBs. Tension is applied in the simulation at a strain rate of 10^{10} s^{-1}; the high strain rates are indicative of MD. We consider uniaxial tension perpendicular to the GB, while multiaxial loading is left for future research. The atomic system is dynamically deformed with an *NPT* ensemble to a predetermined strain along the axis normal to the GBs, ***n***. During the simulation, the positions of the atoms, centrosymmetry parameter per atom [62], Virial stress and energy per atom are measured and dumped per a time-step increment. Visual molecular dynamics (VMD) is used to visualize the simulation [63]. In addition, the centrosymmetry parameter is utilized to locate and color the defects within the material based on its position with respect to its nearest neighbors (red indicates a partial dislocation, while gold denotes a stacking fault). For clarity, defect-free atoms that do not participate in the interaction are deleted from the MD simulation snapshots.

3. Results

The energy, E^{GB}_{CSL}, of *N* atoms containing the pair of CSL GBs was measured by relaxing the system. The energy associated with the grain boundary was calculated by the following:

$$E^{GB}_{Static} = \frac{E^{GB}_{CSL} - \frac{N}{M} \cdot E^{fcc}_{Perfect}}{2A}, \tag{3}$$

where *A* is the area of the GB ($B \cdot W$) and the factor of 2 is necessary since the system contains two GBs. In order to isolate the GB energy, we must remove the potential energy of the atoms in the lattice, $E^{fcc}_{Perfect}$ (4.45 eV per *M* atoms). The simulation was repeated for various rotations about the ⟨1 1 0⟩ tilt, ⟨1 1 1⟩ twist and ⟨0 0 1⟩ axes, and the results are shown in Fig. 3. It can be seen that the ⟨1 1 0⟩ tilt GB curve contains local minima and cusps corresponding to

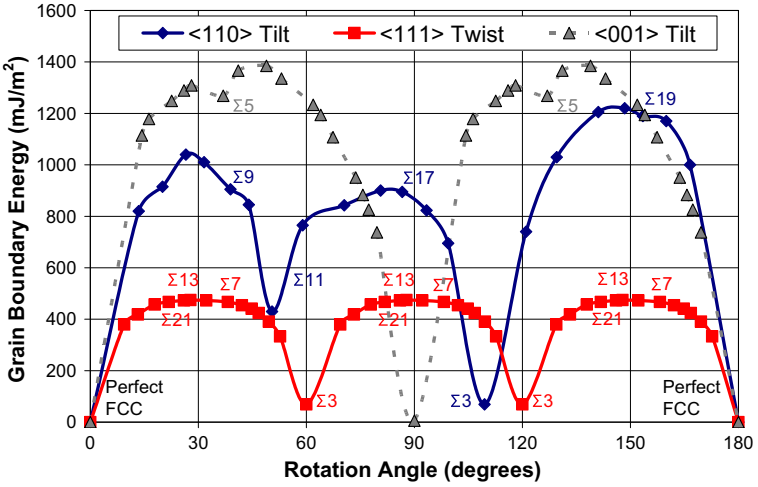

Fig. 3. The grain boundary energy shown as a function of the rotation angle for nickel in the ⟨1 1 0⟩ tilt, ⟨1 1 1⟩ twist, and ⟨0 0 1⟩ tilt directions.

preferred energy configurations as a result of the special Σ GBs in the CSL, which concurs with simplified defect structures at the interface. At a rotation of 0°, the atoms are in a perfect lattice configuration. At a rotation of 50.48°, the defect structure at the interface is simple, and therefore corresponds to a local minimum in the energy and the Σ11 GB. A 109.47° tilt rotation about the ⟨1 1 0⟩ axis has the lowest energy of any GB, which corresponds to a very simple defect structure known as a coherent twin boundary, also known as a Σ3 GB; this same boundary can also be obtained via a 60° or 120° twist rotation about the ⟨1 1 1⟩ axis. The local cusps at 36.9° tilt rotation about the ⟨0 0 1⟩ axis correspond to the Σ5 GB.

As mentioned above, the strengthening behavior of each GB was observed by deforming the simulation box. This resulted in a partial dislocation nucleating from the void and traveling along a {1 1 1} plane until it reached the GB. In each case the GB acts as a barrier to impede dislocation motion. An example of such a reaction is shown for the case of a coherent twin or Σ3 GB in Fig. 4a. For this case, the system is loaded in the [1 1 1] orientation and the incident dislocation is comprised entirely of an edge component; hence the dislocation reaction is two-dimensional and chosen for clarity. The trailing partial is pinned at the source, resulting in a stacking fault in the wake of the dislocation. Since the loading is perpendicular to the GB, the Schmid factor of the coherent twin boundary is zero. As shown by the reaction in Fig. 4b, the high stability and coherency of the twin boundary forces the dislocation to transmit the GB on a non-Schmid, cubic {1 1 1} plane, thus nucleating a Lomer-type dislocation which glides in the adjacent grain. For this loading configuration, the highest Schmid factor, 0.47, is obtained on the (1 0 0) cube plane resulting in a maximum value of the critical resolved shear stress, 8 GPa, on the transmitted dislocation. In this case, there is no resolved shear stress on the GB and the system is loaded uniaxially in the [1 1 1] direction, thus no other glissile slip systems are available leading to cubic slip penetration. This phenomenon has been observed by others in experiments (at room temperature of low stacking fault fcc alloys) [64,65] and in MD simulations [51,66]. In the presence of a resolved shear stress at the GB, however, slip transmission occurs on a glide plane [66].

To grasp the role of the GBs on the energetics of each system, a contour plot was created of the potential energy of each atom during the slip–GB interaction. The potential energy is governed by the spatial packing of the crystal; hence the introduction of defects and slip–GB interactions affects their position and potential energy. A cross-sectional view of the contour energy plot for an incident dislocation interacting with a Σ3 GB is shown in Fig. 5; this corresponds to the same reaction observed in Fig. 4. It can be seen that the atoms around the void have higher energy due to a deficient number of nearest neighbors. Upon loading, a dislocation nucleates from the void, which is discernible by a heterogeneous rise in energy. The leading partial dislocation propagates towards the GB resulting in a stacking fault. During interaction, the dislocation is

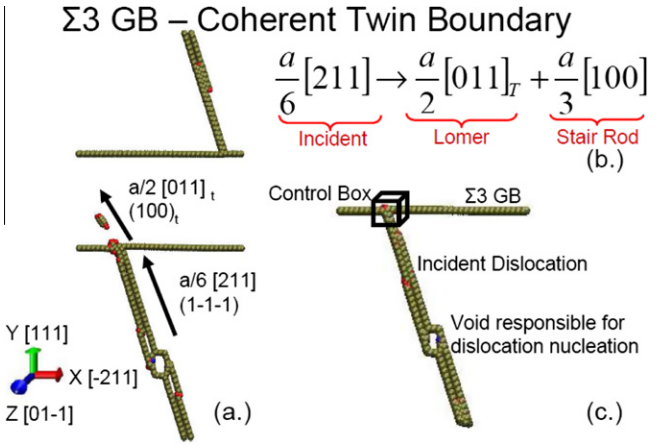

Fig. 4. (a) Dislocation–Σ3 GB (coherent twin) interaction and (b) the resulting dislocation reaction. Please note that, for clarity, only the atoms representing defects are shown. In this system, a void is introduced to facilitate dislocation nucleation. (c) Schematic of a control box surrounding the atoms involved in the slip–Σ3 GB interaction.

impeded as the energy in the vicinity of the interaction increases until it is sufficiently large to allow the dislocation to transmit to the adjacent grain. In this case, it corresponds to nucleation of a Lomer dislocation at the interaction site. Local variations in the energy are small and nearly insignificant. It is possible to calculate the energy barrier for dislocation–GB interaction by viewing a control box around the interaction, as shown in Fig. 4c.

To date, the vast majority of MD studies provide qualitative behavior into the mechanics of materials. Our goal is to understand quantitatively the atomistics of GBs using MD. Hence, a control box is placed at the intersection of the dislocation and GB. In each case, the control box is only placed along the atoms which play a role in the interaction; hence it is not a simple cubic box. This process consists of writing codes to view the simulation using VMD of the defects identified by the centrosymmetry parameter, where definitions of stacking faults ($P = 4.0$–20.0, colored green), partial dislocations ($P = 0.5$–4.0, colored red), and non-defect atoms ($P < 0.5$, atoms removed from atomistic snapshots) are in accordance with Ref. [62]. As the dislocation moves through the simulation and interacts with the GB, all the defect atoms in the reaction identified by the centrosymmetry parameter are included in the control box. Extreme care is taken to select the positions of only the relevant defect atoms, and then running a Matlab algorithm that selects these atoms and measures their energy:

$$E_{Barrier} = \frac{\sum_i^n E_{load}^i - E_{static}}{volume}, \tag{4}$$

where for each atom i within the control box, the energy upon loading of that atom, E_{load}^i, is reduced by the energy of that atom in its static relaxed position, E_{static}, and normalized by the volume of the control box. The control box can be partitioned into a series of parallelepipeds and the volume of the control box is equivalent to the sum of the parallelepiped's volumes. Midpoints between the atoms at the outskirts (i.e. surface) of the control box and their nearest neighbors of non-defect atoms are determined in the *x*-, *y*- *and* *z*-directions. The volumes of the partitioned parallelepipeds are determined from the boundary of the control box via the construction of these midpoints. The result of Eq. (4) produces the energy barrier for slip–GB interaction in units of mJ m^{-3}. This process is dependent on the size of the control box, and hence only the atoms contributing to the reaction must be included and monitored. Furthermore, for the cases of a residual dislocation incorporated within the GB plane, the control box must also include the spreading and dissociation of the dislocation within the boundary.

In order to verify our new method for determining the energy barrier, a system was constructed without a GB. In this case, the dislocation nucleated from the void and the control box measured the lattice resistance to slip in a perfect fcc crystal. For such a case, the energy was measured according to Eq. (4) and multiplied by the slip length within the control box, ζ, to obtain the energy barrier in terms of the fault energy per unit area. The result of this was compared to the GSFE calculated from molecular statics, ab initio calculations [60] and experiments, as shown in Fig. 6. There was only a 6% difference between the MD control box method and the relaxed GSFE curve, thus validating our method. In these simulations, a trailing partial was not produced; hence the second barrier of the control box curve is represented by a dashed line.

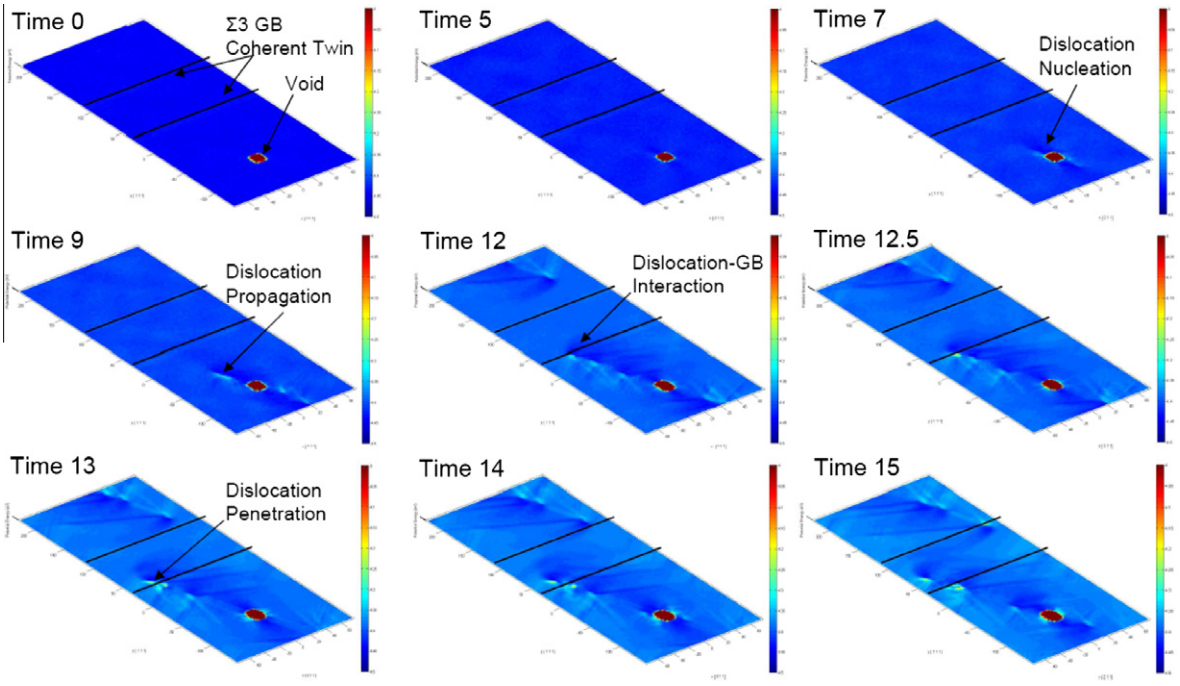

Fig. 5. Cross-sectional view of a contour plot of the energy (in units of eV) for the reaction shown in Fig. 4 for various simulated time-steps.

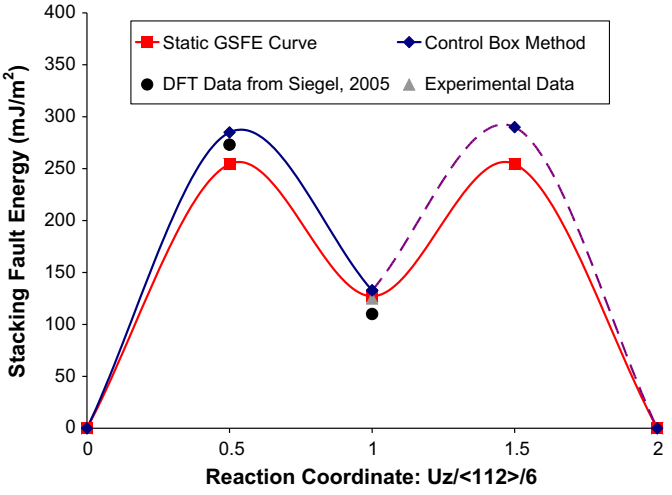

Fig. 6. Verification of the method for measuring the energy barrier to slip in a perfect fcc material by placing a control box around a set of atoms and measuring the energetics during a MD simulation. This is compared to values from experiments, density functional theory [60] and the molecular statics response, where the atoms are allowed to fully relax. The dynamic calculation is less than 6% different than the static curve.

The slip–GB reactions were observed for various types of GBs: ⟨1 1 0⟩ tilt – Σ3, 9, 11, 17, and 19; ⟨1 1 1⟩ twist – Σ3, 7, 13, and 21; ⟨0 0 1⟩ tilt – Σ5; and perfect fcc material. In each reaction, the incident leading partial dislocation glides along a {1 1 1} plane and interacts with the GB as shown in Fig. 7a–c for Σ3, Σ7 and Σ11 GBs, respectively. As shown in Fig. 7b and c, the incident dislocation is typically a loop containing mixed screw and edge components. After interaction with the GB, a partial is transmitted into the adjacent grain on a glissile Schmid {1 1 1} plane. Slip–Σ11 GB interaction results in a residual dislocation absorbed in the boundary plane as shown in Fig. 7c by the red[1] loop within the GB, indicating a partial dislocation. The resulting energy barriers for slip to penetrate the GBs are shown in Fig. 7d–f for Σ3, Σ7 and Σ11 GBs, respectively. In each case, local fluctuations in energy are observed as the system is loaded corresponding to vibrations of the atoms via a temperature thermostat. These fluctuations are small compared to the energy barriers. Also, prior to interaction, the elastic strain energy of the material is removed from the energy barrier plots. The systems are loaded to a predetermined strain; meanwhile the energy plots are linked to the visualization of the system, which indicate dislocation nucleation from the source and dislocation interaction with the GB. In each simulation, the dislocation nucleates at various applied strains due to the differences in the loading axis. After the dislocation interacts with the GB, the energy significantly rises to a maximum value and decreases after slip is transmitted into the adjacent grain. This value is taken as the energy barrier for slip transmission across a GB. It can be seen that the coherent twin boundary (Σ3 GB) provides a greater energy barrier to slip than the Σ7 and Σ11 GBs.

By removing the void and placing the control box along the entire GB, we can also measure the energy barrier for dislocation nucleation from a GB. This process was repeated for the same types of GBs as previously mentioned: ⟨1 1 0⟩ tilt – Σ3, 9, 11, 17, and 19; ⟨1 1 1⟩ twist – Σ3, 7, 13, and 21; ⟨0 0 1⟩ tilt – Σ5; and perfect fcc material. From this analysis, the dislocation emission from Σ5, Σ9, and Σ19 GBs is shown in Fig. 8a–c, respectively. In each case, to satisfy compatibility of the system during the applied deformation, dislocations are nucleated from the GBs on a glissile Schmid {1 1 1} plane. A single dislocation loop of mixed edge and screw components representing a leading partial is emitted for the Σ5 and Σ9 GBs, as shown in Fig. 8a and b. For the case of nucleation from a Σ19 GB, the dislocations are emitted in a homogeneous manner as the intrinsic stacking fault facets extend from the GB. The dissociation of the GB corresponds to the structural units that comprise the static GB, which is in agreement with the literature [39].

The corresponding energy barriers to dislocation emission for the previous cases, Σ5, Σ9 and Σ19 GBs, are shown in Fig. 8d–f, respectively. In each case, the energy of the atoms within the control box, i.e. the GB interface region, increases until nucleation of the first dislocation. At this point, the system can relax around the dislocation and the energy decreases. The result is an energy barrier to dislocation emission. These plots include the strain energy density as this contributes to dislocation nucleation. From the examples shown, the Σ9 GB offers the highest barrier to dislocation nucleation, while the Σ19 GB has the lowest energy barrier. For the cases of a dislocation nucleating from Σ3 GB, Σ11 GB and perfect fcc material, these systems have a simple dislocation structure and stable configurations. Hence, in these simulations, dislocations are emitted in the matrix material, preventing a measurement of the energy barriers to nucleation.

4. Discussion

To our knowledge, this study represents the first time the energy barriers preventing slip from penetrating a GB (Fig. 7) or nucleating from a GB (Fig. 8) have been measured from a control box of atoms pertinent to the interaction. This process is repeated for relevant GBs and the energy barrier results for slip interaction and slip penetration are calculated. We rationalized the energy barriers for various types of GB with their static GB energy; these results are shown in Fig. 9 as the energy barrier to slip transmission across a GB plotted against the static GB energy for each GB. For each type of GB, there is an inverse relationship between the energy barrier to slip and the static energy for each GB. A power-law function was fit to the data, resulting in the following:

$$E_{Barrier}^{Transmission} = 2.8 \times 10^{13} \cdot \left(E_{Static}^{GB}\right)^{-0.6}, \quad (5)$$

[1] For interpretation of color in Figs. 1–9 and 11–14, the reader is referred to the web version of this article.

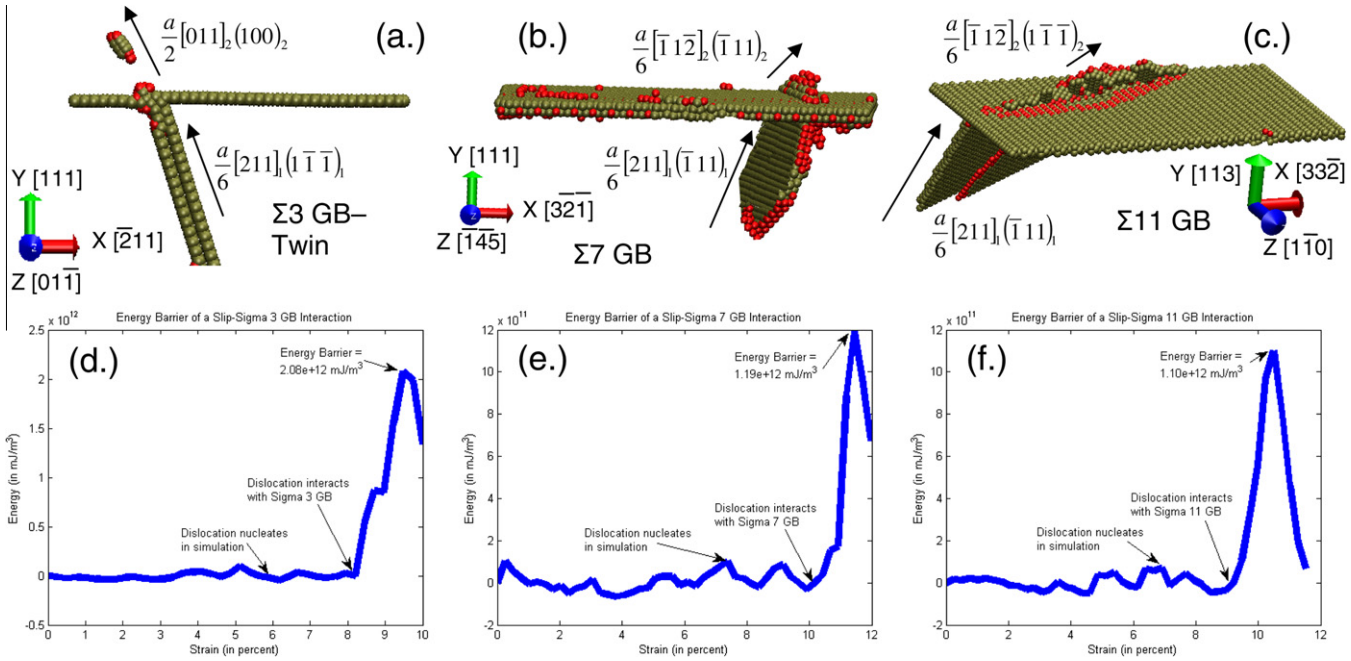

Fig. 7. Interactions of dislocations with (a) Σ3 GB (coherent twin), (b) Σ7 GB and (c) Σ11 GB with the resulting dislocation reactions; and the corresponding energy barrier calculations for slip to penetrate the (d) Σ3 GB (coherent twin), (e) Σ7 GB, and (f) Σ11 GB, in terms of the energy barrier within the control box as calculated by Eq. (4) to the overall applied strain to the simulated system.

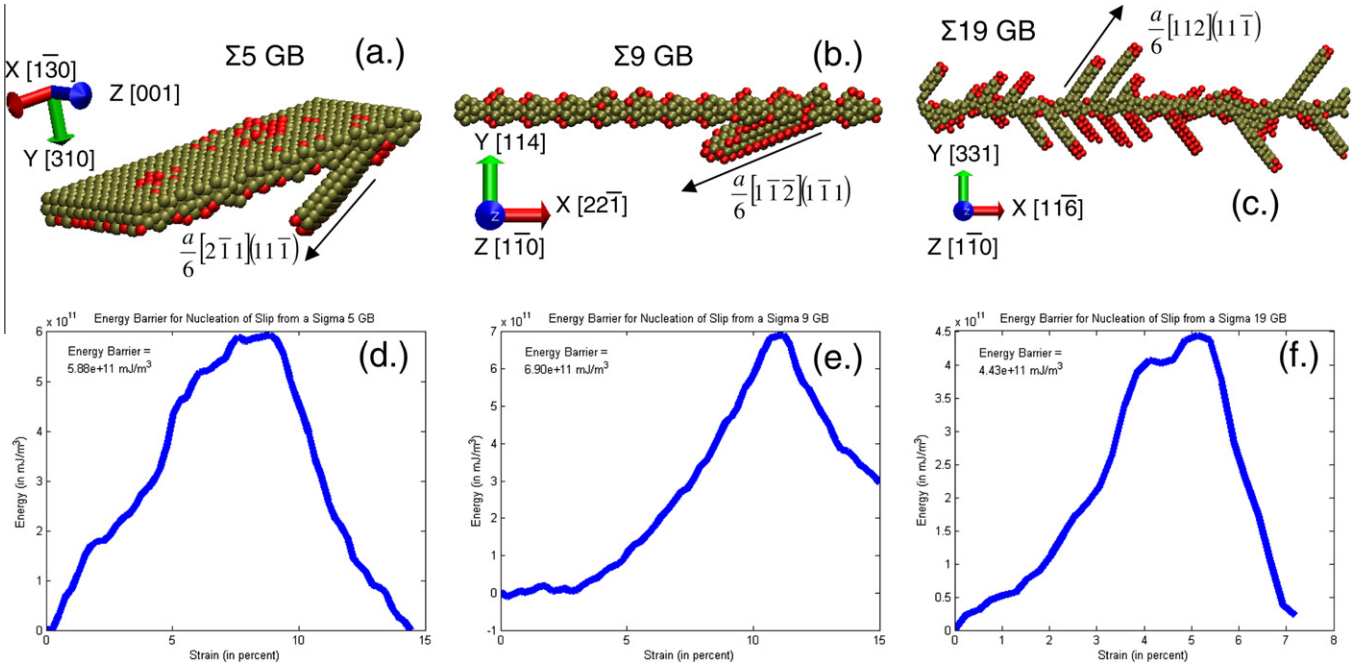

Fig. 8. Nucleation of dislocations from (a) Σ5 GB, (b) Σ9 GB and (c) Σ19 GB with the direction and plane of the emitted dislocation; and the corresponding energy barrier calculations for dislocations to nucleate from the (d) Σ5 GB, (e) Σ9 GB and (f) Σ19 GB, in terms of the energy barrier within the control box as calculated by Eq. (4) to the overall applied strain to the simulated system.

where the static GB energy, E^{GB}_{Static} (units of mJ m^{-2}), and the GB energy barrier to slip transmission, $E^{Transmission}_{Barrier}$ (units of mJ m^{-23}), are the same quantities measured in Eqs. (3) and (4), respectively. This relation is only valid for GBs in the range of the simulation data.

As expected, the perfect fcc material does not provide a strong barrier against slip, as this represents a perfect crystal and thus only lattice resistance to flow. The energy barrier for slip in a perfect fcc lattice agrees with the GSFE of the material. Hence, we have validated that the energies

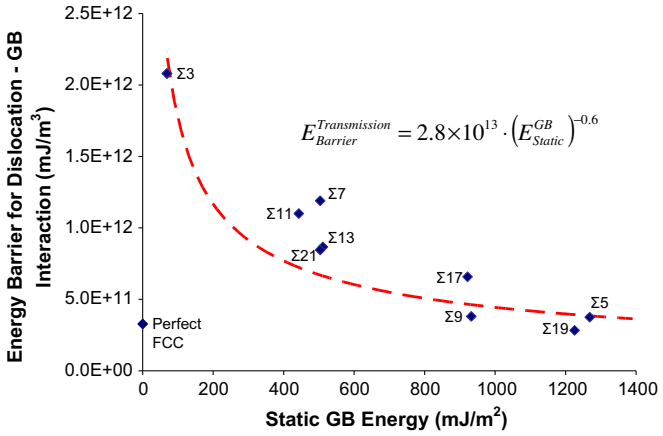

Fig. 9. Energy barriers for slip to penetrate a GB plotted against the static GB energy for various types of CSL GBs. There is a relationship between the static GB energy and GB energy barrier to slip as shown by the power-law fit of the data.

calculated are accurate. The coherent twin boundary–Σ3 GB offers the lowest interface energy and highest barrier to slip, thus providing a significant strengthening contribution. As previously shown (Fig. 4), the Σ3 GB transmits a Lomer dislocation in the cube plane within the adjacent grain. Since this is not a close-packed plane, the energy barrier to slip along this plane is significantly higher. In order to compare the energy barriers associated with different GBs, we have normalized the value to the energy per volume. By multiplying this value by the slip length (distance traveled to traverse the GB or the Burgers vector's magnitude to nucleate a dislocation), we see that the energy barriers are consistent with the GSFE and the different levels of barrier heights expected based on the known difficulty of penetrating different GB types [19] (a coherent twin boundary is a strong barrier against slip compared to the material's lattice resistance (perfect fcc)).

Experimental evidence for the dislocation reactions with high-angle boundaries is very complex. There have been numerous experimental and analytical studies detailing slip–twin interactions [67,68], since the static dislocation structure at the GB is simplest for a coherent twin, Σ3, boundary [31–33]. CSL GBs with $\Sigma > 3$ values have more complex static defect structures at the GB [31–33], hence the dislocation reactions are far more complicated for $\Sigma > 3$ GBs compared with twins (Σ3), which explains the dearth of analytical models. In the last 10 years, MD simulations have proven to be valuable in predicting these complex reactions for cases where experimental evidence is lacking. Examples shown in the literature do not provide quantitative values for energy barriers, although we observe the same type of dislocation reactions in our MD simulations compared with available cases in the literature.

Similar dislocation reactions were observed via in situ TEM analysis of a low stacking fault material (310 stainless steel). As shown in Figs. 10–12, incident dislocations interact with the GB resulting in dissociation into an outgoing dislocation and a residual dislocation within the GB. Fig. 10a displays a Σ3, twin, boundary, whereas the incoming dislocations are initially impeded by the GB, resulting in a dislocation pile-up. Hence, the Σ3 boundary offers a strong barrier to slip. As the applied load is increased, dislocations eventually traverse the GB, leaving behind a residual dislocation within the GB (Fig. 10b), which is in agreement with our MD simulations (Fig. 5).

Experimental observation of slip transmission through a Σ13 GB is shown in Fig. 11a and compared to the simula-

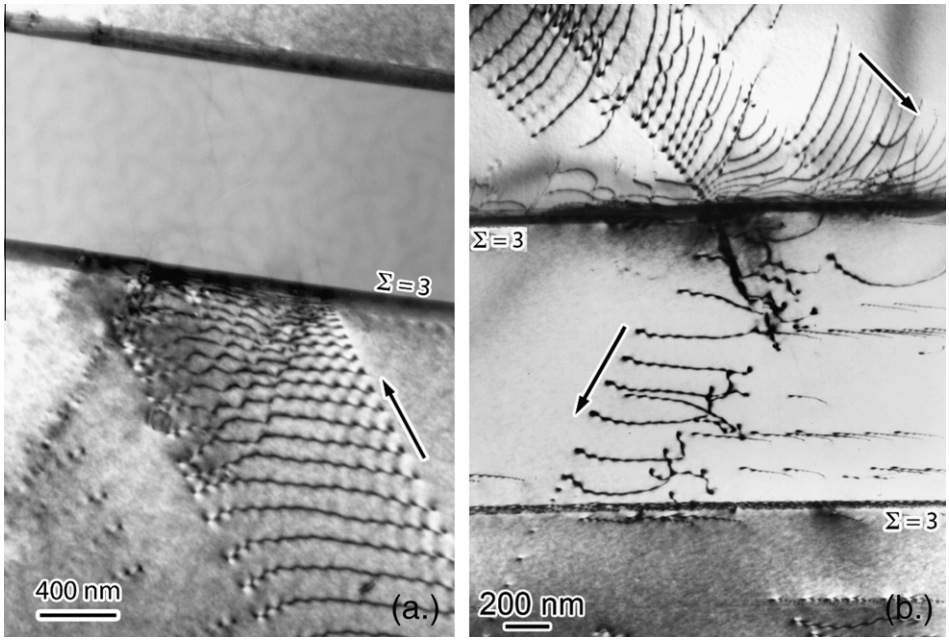

Fig. 10. In situ TEM micrograph of slip in a low stacking fault energy material Σ3 (twin) boundaries. (a) Slip is initially impeded by the twin resulting in a dislocation pile-up. (b) As the applied load increases, slip transmits past the twin boundary.

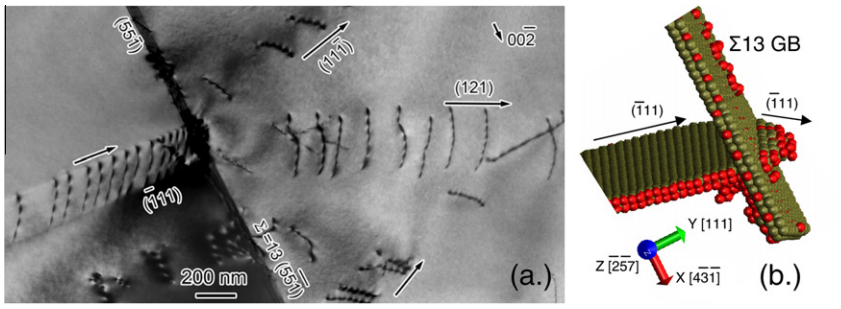

Fig. 11. (a) In situ TEM micrograph of slip transmission in a low stacking fault energy material for a Σ13 GB. This micrograph is a composite figure formed from images in which the diffraction condition was specific to each grain and based on Ref. [20]. (b) MD simulations of slip transmission through a Σ13 GB. The simulated slip–Σ13 GB interaction compares well with the experimental results.

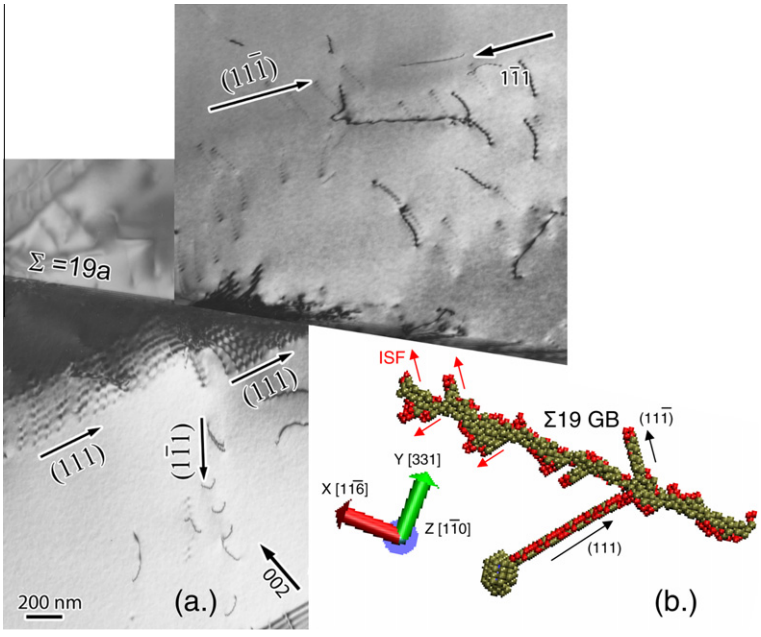

Fig. 12. (a) In situ TEM micrograph of slip transmission in a low stacking fault energy material for a Σ19 GB. This micrograph is a composite figure formed from images in which the diffraction condition was specific to each grain and based on Ref. [20]. (b) Slip–Σ19 GB reaction resulting in slip transmission. In addition, the Σ19 GB is comprised of intrinsic stacking faults (ISFs), which extend during loading (as shown in Fig. 8c and the TEM image in figure a). Equivalent reactions are observed between experiment and simulation.

tion results in Fig. 11b. In both cases, the plane of the incident dislocation is the same, and the reaction results in a residual dislocation within the GB and slip transmission through the GB. The experimental and simulation results are similar for the Σ13 GB, although the GB plane is different in the two cases and consequently different outgoing dislocation planes are observed. A comparison between experimental and simulation results for slip–Σ19 GB interactions is presented in Fig. 12. In both cases, we observe dislocation transmission through the GB with the incident dislocation dissociating into a residual dislocation absorbed in the GB. From the analysis, we see excellent agreement between experiments and simulations, whereas the overall reactions as well as the incident/outgoing dislocation planes are the same. The Σ19 GB is composed of intrinsic stacking faults (ISFs), which lengthen during loading. This behavior is observed in both the simulations and experiments as stacking faults extend from the GB. The ISFs have an associated stress field, which interacts with the stress field produced by the incident dislocation. Consequently, these stress fields lower the energy barrier for slip transmission through this boundary, thus explaining the negligible difference between slip through a Σ19 GB and a perfect fcc lattice, as shown in Fig. 9.

Each simulated case of slip transmission agreed with the reactions outlined in Refs. [9,19] and the LRB strain incompatibility criteria (composed of three conditions) for strain incompatibility across a GB [7]. The first is a geometrical condition for predicting the active slip plane by minimizing the angle between the lines of intersection (l) of the incident/outgoing slip planes to the GB, thus maximizing M:

$$M = l_{in} \cdot l_{out}. \tag{6}$$

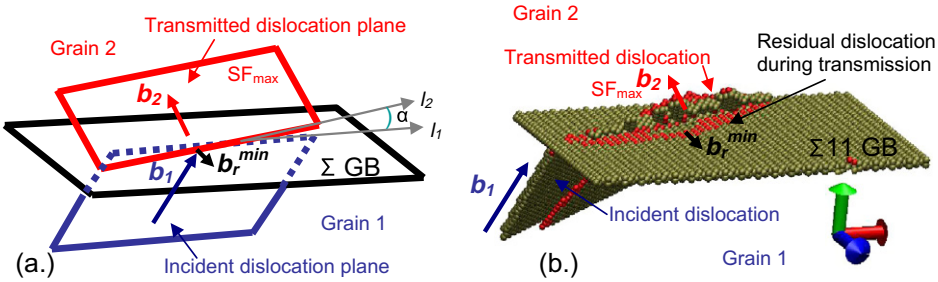

Fig. 13. (a) Schematic of slip transmission through a GB displaying the LRB criterion; whereas the angle between the lines of intersection (slip plane – GB plane) must be minimized, the resolved shear stress on the outgoing slip system must be maximized (SF_{max}), and the residual dislocation within the GB must be minimized. (b) MD results of slip transmission through a Σ11 GB. The simulation is in agreement with the LRB criterion, as shown in Table 2.

The second part of the criterion determines the slip direction based on the maximum resolved shear stress on the active slip plane. The third condition requires a Burgers vector of the residual dislocation (difference in $\boldsymbol{b}$ of incoming and outgoing dislocation) to be minimized:

$$\vec{b}_{res} = \vec{b}_{in} - R'_{12} \cdot \vec{b}_{out}, \tag{7}$$

where R_{12} is the misorientation tensor between grains 1 and 2. A schematic displaying each of the three criteria is shown in Fig. 13a. In each slip–GB reaction investigated in this study, the results agreed with these LRB criteria.

An example is shown for the case of transmission through a Σ11 GB as the active outgoing slip system is $\frac{a}{6}[\bar{1}\,1\,\bar{2}]_2(1\,\bar{1}\,\bar{1})_2$ (Fig. 13b). The geometric condition is satisfied as the angle, α, is minimized, as we have specifically checked all four slip planes for each of the potential outgoing dislocations. As shown in Table 2, the geometric condition yields a 0° angle between the lines of intersects between the GB and the ingoing/outgoing planes. Once the active slip planes are chosen, the direction is calculated based on maximizing the resolved shear stress, resulting in a Schmid factor for this system of 0.47 for the Σ11 GB (Table 2). As a result, the critical resolved shear stress on the transmitted dislocation is 4.8 GPa. Burgers vector analysis of the simulation results reveal that the residual dislocations are in the form of either a stair rod or Frank dislocation and are minimized in all cases. This is confirmed through a computational investigation of the MD simulations [66] and analytically from the incident and outgoing dislocation reactions (Eq. (7)). For the Σ11 GB, the residual Burgers vector at the GB is minimized, which was calculated to be $0.41a[1\,0\,\bar{1}]$ for the active slip systems. The results of the LRB criteria calculations are shown in detail for the Σ11 GB in Table 2, and are in perfect agreement with the simulation results for the Σ11 GB, as shown in Fig. 13b.

Similarly, the energy barrier for slip nucleation from a GB is plotted against each GB's static energy, as shown in Fig. 14. Once again, there is an inverse relationship between the static GB energy, E^{GB}_{Static} (Eq. (3), units of mJ m^{-2}), and the GB energy barrier to slip nucleation, $E^{Nucleation}_{Barrier}$ (Eq. (4), units of mJ m^{-3}), as shown by the power-law fit:

$$E^{Nucleation}_{Barrier} = 6.0 \times 10^{15} \cdot (E^{GB}_{Static})^{-1.3}. \tag{8}$$

As previously mentioned, due to the stability of the GBs, the energy barrier to dislocation nucleation could not be measured for GBs with low interfacial energy, as indicated in Fig. 14 by the gray vertical line. Due to their stability, in the simulation, dislocations nucleated within

Table 2
Prediction of the activated slip system for transmission through a Σ11 GB. In this case, the loading direction is [0,0,1] and the incident slip is of $\frac{a}{6}\langle 2\,1\,1\rangle_1(\bar{1}\,1\,1)$ type, resulting in a line of intersection, $l_1 = [-0.8, 0, 0.2]$. Slip transmission follows the LRB criterion for strain incompatibility [7]. Each of these conditions is satisfied here. From this analysis, the LRB predictions match the MD simulation results.

Condition	Geometric			Resolved shear stress	Residual GB dislocation
Outgoing slip system	l_2	α (degree)	M	Schmid factor	$\boldsymbol{b}_r$
$\frac{a}{6}[\bar{1}\,2\,\bar{1}]_2(1\,1\,1)_2$	[0, 0, 0.5]	73.2	0.12	0	$0.41a[1\,\bar{1}\,0]$
$\frac{a}{6}[2\,\bar{1}\,\bar{1}]_2(1\,1\,1)_2$	[0, 0, 0.5]	73.2	0.12	0	$0.82a[2\,1\,0]$
$\frac{a}{6}[\bar{1}\,\bar{1}\,2]_2(1\,1\,1)_2$	[0, 0, 0.5]	73.2	0.12	0	$0.41a[1\,2\,3]$
$\frac{a}{6}[1\,2\,1]_2(\bar{1}\,1\,\bar{1})_2$	[0.8, 0, 0.2]	146.4	−0.61	0.24	$0.41a[3\,\bar{1}\,2]$
$\frac{a}{6}[1\,\bar{1}\,\bar{2}]_2(\bar{1}\,1\,\bar{1})_2$	[0.8, 0, 0.2]	146.4	−0.61	0.47	$0.41a[3\,2\,\bar{1}]$
$\frac{a}{6}[\bar{2}\,\bar{1}\,1]_2(\bar{1}\,1\,\bar{1})_2$	[0.8, 0, 0.2]	146.4	−0.61	0.24	$0.82a[0\,1\,1]$
$\frac{a}{6}[\bar{1}\,1\,\bar{2}]_2(1\,\bar{1}\,\bar{1})_2$	[−0.8, 0, 0.2]	0	0.73	0.47	$0.41a[1\,0\,\bar{1}]$
$\frac{a}{6}[2\,1\,1]_2(1\,\bar{1}\,\bar{1})_2$	[−0.8, 0, 0.2]	0	0.73	0.24	$0.82a[2\,0\,1]$
$\frac{a}{6}[\bar{1}\,\bar{2}\,1]_2(1\,\bar{1}\,\bar{1})_2$	[−0.8, 0, 0.2]	0	0.73	0.24	$0.41a[1\,3\,2]$
$\frac{a}{6}[\bar{2}\,1\,\bar{1}]_2(\bar{1}\,\bar{1}\,1)_2$	[0, 0, −1]	106.8	−0.24	0	–
$\frac{a}{6}[1\,\bar{2}\,\bar{1}]_2(\bar{1}\,\bar{1}\,1)_2$	[0, 0, −1]	106.8	−0.24	0	$1.22a[1\,1\,0]$
$\frac{a}{6}[1\,1\,2]_2(\bar{1}\,\bar{1}\,1)_2$	[0, 0, −1]	106.8	−0.24	0	$1.22a[1\,0\,1]$
Criterion value	–	**0**	**0.73**	**0.47**	$0.41a[1\,0\,\bar{1}]$

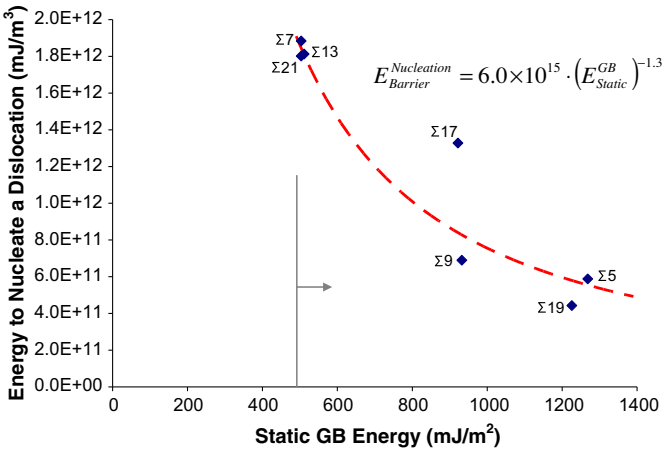

Fig. 14. Energy barriers for slip to nucleate from a GB plotted against the static GB energy. There is a relationship between the static GB energy and GB energy barrier to dislocation nucleation as shown by the power-law fit of the data. To the left of the gray solid line, the energy barriers cannot be measured, since the Σ1 (perfect fcc), Σ3 (coherent twin) and Σ11 GBs have a simple dislocation structure and stable configurations. Hence dislocations were nucleated in the matrix material during the simulation, preventing the energy barrier calculations.

the matrix material as opposed at the Σ3 and Σ11 GBs. Hence, the above relationship is only valid to the right of the gray vertical line in the range of the simulation data.

Recently, during the onset of plastic deformation in pure metals and alloys, GBs have been recognized as the principal source for dislocations [69,70]; this includes an in situ TEM study [21], in which a low-energy CSL (Σ9) GB required significantly higher stress to emit a dislocation compared to other general types of boundaries tested in this study. This further validates our findings that low-energy GBs require higher stresses and activation energies to nucleate dislocations compared to inherently less stable, higher-energy GBs.

The energy barriers associated with dislocations nucleating from a GB (Fig. 14) are higher compared to those transmitting through a similar GB (Fig. 9). There is an associated stress–strain field with the incident dislocation, which acts to lower the energy barrier necessary for dislocation transmission through the GB. In cases of nucleation, the material surrounding the GB is pristine; hence it requires more energy to emit a dislocation into the perfect matrix material.

The energy barriers reported in this paper were calculated for Ni, although the trends should hold for fcc materials and scale according to the GSFE values [71]. The simulations have been verified at higher temperatures (300 K) and lower strain rates (10^8 and 10^9 s^{-1}) as the resulting dislocation reactions were consistent at each of these various test parameters. At higher temperatures, the local fluctuations in energies are more significant. Since the control box method is a local method, we needed to ensure minimal fluctuations, and hence a low temperature was chosen. We contend that the dislocation reactions in our analyses and room temperature experiments are in conformity; consequently our calculated energy barriers are accurate. Additionally, we show nearly perfect agreement with the GSFE, which is strain rate independent. Further study is needed to investigate scaling the energy barrier results with temperature and strain rate as discussed by Deng and Sansoz [72] and earlier by Zhu et al. [54], although we point out the focus is on the diversity of GBs presented in this paper.

Based on the results of this investigation, the slip–GB interaction is strongly dependent on the geometry of the bicrystal system applied loading orientation, the Schmid factor of the interface and the GB structure. The applied loading and Schmid factor play an important role in the kinetics of the dislocation behavior. The geometry and GB structure determine the static GB energy according to the structural units of the defects at the interface [31–33]. This plays an important role in the transmission and nucleation processes. As can be seen in Figs. 8c and 12b, a GB with a dissociated structure results in the growth of intrinsic stacking faults during loading. From afar, this can be viewed as nearly homogeneous nucleation. As a consequence, the energy barrier for nucleation and transmission from a GB exhibiting a dissociated structure is significantly lower. This is in direct opposition to the simple defect structures, i.e. Σ3 and Σ11 GBs, which have a low static GB energy and offer a substantial barrier to dislocation transmission.

From these measurements of the energy barriers, we can draw a quantitative description of each GB's impact on the strengthening behavior of a material, thus providing a powerful contribution to the kinetics of slip. These energy barriers have direct implications to the field of material modeling, specifically crystal plasticity, fatigue, fracture and creep. Which until now, the energy barriers were assumed values (fitted or back-calculated constants), in this work, we do not make such assumptions, thus offering significant progress in the field. We accurately compute the energy barriers associated with slip nucleation and transmission at GBs for non-static cases. This information provides a valuable contribution, since we can more accurately interpret the role of each GB on the impedance of deformation.

5. Conclusions

Molecular dynamics simulations are used to study the slip–GB interactions, including strain transmission and dislocation nucleation at a GB. The aim of this work is to quantify the strengthening mechanisms of individual GBs. Significant contributions of this study are summarized as follows:

1. A new methodology is introduced to measure energy barriers based on placing a control box around the pertinent defect atoms. By tracking the atom position and their corresponding energies, during the interaction, it is possible to obtain the energy barrier for slip transmission or nucleation at a GB. This methodology is validated by comparing the energy barrier of slip in a

perfect fcc material to the general static fault energy curve; the results displayed a modest 6% difference.

2. The energy barriers for slip transmission are calculated across various classifications of GBs: ⟨1 1 0⟩ tilt – Σ3, 9, 11, 17, 19; ⟨1 1 1⟩ twist – Σ3, 7, 13, 21; and ⟨0 0 1⟩ tilt – Σ5. Each reaction is in agreement with experimental observations of slip transmission and the LRB criterion for strain incompatibility, which is specifically illustrated for the Σ11 GB by surveying all outgoing dislocation scenarios. The coherent twin (Σ3) boundary provides the highest barrier for slip transmission, while boundaries such as the Σ13 and Σ19 provide lower resistance to transmission. This is demonstrated by favorable comparisons of trends in dislocation behaviors between simulations and in situ TEM.
3. The energy barriers to dislocation nucleation from the aforementioned GBs are calculated. The Σ3 and Σ11 GBs have a stable configuration, hence nucleation from the GB is not observed in the simulation. Upon loading of GBs with dissociated structures, the intrinsic stacking fault regions extended in a periodic manner across the interface. Hence, the nucleation event was nearly homogeneous, resulting in a lower energy barrier.
4. The energy barrier from the slip–GB interaction is significantly affected by the character and the structure of the GB, as there is a strong correlation between the energy barrier and interfacial boundary energy. GBs with lower static interfacial energy offer a stronger barrier against slip transmission and nucleation at the GB. Experimental observations support these findings as demonstrated in this study.

Acknowledgements

Support for this work was provided by Rolls-Royce Corporation and the National Science Foundation, DMR Grant No. 0803270. The authors would like to acknowledge Dr. Stephen M. Foiles of Sandia National Laboratory for sharing his nickel EAM potential. I.M.R. acknowledges support of DOE BES through Grant DEFG-02-07ER46443.

References

[1] Hirth JP. The influence of grain boundaries on mechanical properties. Metall Trans A Phys Metall Mater Sci 1972;3:3047.
[2] Hall EO. The deformation and ageing of mild steel III. Discussion of results. Proc Phys Soc Sect B 1951;64:747.
[3] Petch NJ. Cleavage strength of polycrystals. J Iron Steel Inst 1953;26:601.
[4] Kashihara K, Inoko F. Effect of piled-up dislocations on strain induced boundary migration (SIBM) in deformed aluminum bicrystals with originally Σ3 twin boundary. Acta Mater 2001;49:3051.
[5] Livingston JD, Chalmers B. Multiple slip in bicrystal deformation. Acta Metall 1957;5:322.
[6] Shen Z, Wagoner RH, Clark WAT. Dislocation pile-up and grain boundary interactions in 304 stainless steel. Scripta Metall 1986;20:921.
[7] Lee TC, Robertson IM, Birnbaum HK. Prediction of slip transfer mechanisms across grain boundaries. Scripta Metall 1989;23:799.
[8] Hirth JP, Lothe J. Theory of dislocations. New York: Wiley Interscience; 1992.
[9] Sutton AP, Balluffi RW. Interfaces in crystalline materials. Oxford: Oxford Classical Texts; 2006.
[10] Lim LC. Slip–twin interaction in nickel at 573 K at large strains. Scripta Metall 1984;18:1139.
[11] Venables JA. Deformation twinning in face-centred cubic metals. Philos Mag 1961;6:379.
[12] Saito K. Deformation twinning in an age-hardened Cu–4 wt.% Ti alloy. Trans Natl Res Inst Metals 1970;12:158.
[13] Mahajan S, Chin GY. Twin–slip, twin–twin and slip–twin interactions in Co–8 wt.% Fe alloy single crystals. Acta Metall 1973; 21:173.
[14] Remy L. Twin–twin interaction in FCC crystals. Scripta Metall 1977;11:169.
[15] Evans JT. Heterogeneous shear of a twin boundary in α-brass. Scripta Metall 1974;8:1099.
[16] Darby TP, Schindler R, Balluffi RW. On the interaction of lattice dislocations with grain boundaries. Philos Mag A Phys Condens Matter Def Mech Prop 1978;37:245.
[17] Dingley DJ, Pond RC. On the interaction of crystal dislocations with grain boundaries. Acta Metall 1979;27:667.
[18] Lim LC, Raj R. Continuity as slip screw and mixed crystal dislocations across bicrystals of nickel at 573 K. Acta Metall 1985;33:1577.
[19] Shen Z, Wagoner RH, Clark WAT. Dislocation and grain boundary interactions in metals. Acta Metall 1988;36:3231.
[20] Lee TC, Robertson IM, Birnbaum HK. In situ transmission electron microscope deformation study of the slip transfer mechanisms in metals. Metall Trans A Phys Metall Mater Sci 1990;21A:2437.
[21] Kurzydlowski KJ, Varin RA, Zielinski W. In situ investigation of the early stages of plastic deformation in an austenitic stainless steel. Acta Metall 1984;32:71.
[22] Ishida Y, Hasegawa T, Nagata F. Grain-boundary fine structure in an iron alloy. J Appl Phy 1969;40:2186.
[23] Seeger A. Stacking faults in close-packed lattices. Defects in crystalline solids. Bristol: The Physical Society; 1954. p. 328.
[24] Seeger A, Schoeck G. Activation energy problems associated with extended dislocations. Defects in crystalline solids. Bristol: The Physical Society; 1954. p. 328.
[25] Conrad H. The athermal component of the flow stress in crystalline solids. Mater Sci Eng 1970;6:265.
[26] Kocks UF, Argon AS, Ashby MF. Thermodynamics and kinetics of slip. Oxford: Pergamon Press; 1975.
[27] Kocks UF, Tome CN, Wenk H-R. Texture and anisotropy. Cambridge: Cambridge University Press; 2000.
[28] Kocks UF, Mecking H. Physics and phenomenology of strain hardening: the FCC case. Prog Mater Sci 2003;48.
[29] Kronberg ML, Wilson FH. Secondary recrystallization in copper. Am Inst Min Metall Eng J Metals 1949;1:501.
[30] Grimmer H, Bollmann W, Warrington DH. Coincidence-site lattices and complete pattern-shift lattices in cubic crystals. Acta Crystallogr A Crystal Phys Diffract Theor Gen Crystallogr 1974;A30:197.
[31] Sutton AP, Vitek V. On the structure of tilt grain boundaries in cubic metals. I. Symmetrical tilt boundaries. Philos Trans Roy Soc London A Math Phys Sci 1983;309:1.
[32] Sutton AP, Vitek V. On the structure of tilt grain boundaries in cubic metals. III. Generalizations of the structural study and implications for the properties of grain boundaries. Philos Trans Roy Soc London A Math Phys Sci 1983;309:55.
[33] Rittner JD, Seidman DN. ⟨1 1 0⟩ symmetric tilt grain-boundary structures in fcc metals with low stacking-fault energies. Phys Rev B Condens Matter 1996;54:6999.
[34] Yamakov V, Wolf D, Salazar M, Phillpot SR, Gleiter H. Length-scale effects in the nucleation of extended dislocations in nanocrystalline Al by molecular-dynamics simulation. Acta Mater 2001;49:2713.

[35] Froseth AG, Derlet PM, Van Swygenhoven H. Dislocations emitted from nanocrystalline grain boundaries: nucleation and splitting distance. Acta Mater 2004;52:5863.
[36] Spearot DE, Jacob KI, McDowell DL. Nucleation of dislocations from [0 0 1] bicrystal interfaces in aluminum. Acta Mater 2005;53:3579.
[37] Spearot DE, Jacob KI, McDowell DL. Dislocation nucleation from bicrystal interfaces with dissociated structure. Int J Plast 2007;23:143.
[38] Tschopp MA, McDowell DL. Dislocation nucleation in Σ3 asymmetric tilt grain boundaries. Int J Plast 2008;24:191.
[39] Capolungo L, Spearot DE, Cherkaoui M, McDowell DL, Qu J, Jacob KI. Dislocation nucleation from bicrystal interfaces and grain boundary ledges: relationship to nanocrystalline deformation. J Mech Phys Solids 2007;55:2300.
[40] Jin ZH, Gumbsch P, Ma E, Albe K, Lu K, Hahn H, et al. The interaction mechanism of screw dislocations with coherent twin boundaries in different face-centred cubic metals. Scripta Mater 2006;54:1163.
[41] Jin ZH, Gumbsch P, Albe K, Ma E, Lu K, Gleiter H, et al. Interactions between non-screw lattice dislocations and coherent twin boundaries in face-centered cubic metals. Acta Mater 2008;56:1126.
[42] Hoagland RG, Mitchell TE, Hirth JP, Kung H. On the strengthening effects of interfaces in multilayer fcc metallic composites. Philos Mag A Phys Condens Matter Def Mech Prop 2002;82:643.
[43] Hoagland RG, Kurtz RJ, Henager Jr CH. Slip resistance of interfaces and the strength of metallic multilayer composites. Scripta Mater 2004;50:775.
[44] De Koning M, Miller R, Bulatov VV, Abraham F. Modeling the effects of dislocation–grain boundary interactions in polycrystal plasticity: identification and characterization of unit mechanisms, vol. 677. San Francisco (CA): Materials Research Society; 2001. p. AA1.5.1.
[45] De Koning M, Miller R, Bulatov VV, Abraham FF. Modelling grain-boundary resistance in intergranular dislocation slip transmission. Philos Mag A Phys Condens Matter Def Mech Prop 2002;82:2511.
[46] De Koning M, Kurtz RJ, Bulatov VV, Henager CH, Hoagland RG, Cai W, et al. Modeling of dislocation–grain boundary interactions in FCC metals, vol. 323. Les Diableret (Switzerland): Elsevier; 2003. p. 281.
[47] Dewald MP, Curtin WA. Multiscale modelling of dislocation/grain-boundary interactions: I. Edge dislocations impinging on Σ11 (1 1 3) tilt boundary in Al. Modell Simulat Mater Sci Eng 2007;15:193.
[48] Dewald MP, Curtin WA. Multiscale modelling of dislocation/grain boundary interactions. II. Screw dislocations impinging on tilt boundaries in Al. Philos Mag 2007;87:4615.
[49] Cheng Y, Mrovec M, Gumbsch P. Atomistic simulations of interactions between the 1/2(1 1 1) edge dislocation and symmetric tilt grain boundaries in tungsten. Philos Mag 2008;88:547.
[50] Deng C, Sansoz F. Uniaxial compression behavior of bulk nanotwinned gold from molecular dynamics simulation, vol. 1049. Boston (MA): Materials Research Society; 2008.
[51] Afanasyev KA, Sansoz F. Strengthening in gold nanopillars with nanoscale twins. Nano Lett 2007;7:2056.
[52] Van Swygenhoven H, Spaczer M, Caro A. Role of low and high angle grain boundaries in the deformation mechanism of nanophase Ni: a molecular dynamics simulation study. Acta Mater 1998;10:819.
[53] Zhu T, Li J, Samanta A, Kim HG, Suresh S. Interfacial plasticity governs strain rate sensitivity and ductility in nanostructured metals. Proc Natl Acad Sci 2007;104:3031.
[54] Zhu T, Li J, Samanta A, Leach A, Gall K. Temperature and strain-rate dependence of surface dislocation nucleation. Phys Rev Lett 2008;100:025502.
[55] Chen Z, Jin Z, Gao H. Repulsive force between screw dislocation and coherent twin boundary in aluminum and copper. Phys Rev B Condens Matter Mater Phys 2007;75:212104.
[56] Plimpton S. Fast parallel algorithms for short-range molecular dynamics. J Comput Phys 1995;117:1.
[57] Plimpton S. Large-scale atomic/molecular massively parallel simulator. Sandia National Laboratories; 2007.
[58] Sangid MD, Sehitoglu H, Maier HJ, Niendorf T. Grain boundary characterization and energetics of superalloys. Mater Sci Eng A 2010;527:7115.
[59] Foiles SM, Hoyt JJ. Computation of grain boundary stiffness and mobility from boundary fluctuations. Acta Mater 2006;54:3351.
[60] Siegel DJ. Generalized stacking fault energies, ductilities, and twinnabilities of Ni and selected Ni alloys. Appl Phys Lett 2005;87:121901.
[61] Rice JR. Dislocation nucleation from a crack tip: an analysis based on the Peierls concept. J Mech Phys Solids 1992;40:239.
[62] Kelchner CL, Plimpton SJ, Hamilton JC. Dislocation nucleation and defect structure during surface indentation. Phys Rev B Condens Matter 1998;58:11085.
[63] Humphrey W, Dalke A, Schulten K. VMD: visual molecular dynamics. J Mol Graph 1996;14:33.
[64] Karthaler HP. The study of glide on {0 0 1} planes in f.c.c. metals deformed at room temperature. Philos Mag A 1978;38:141.
[65] Korner A, Karthaler HP. Glide dislocations on cube planes in a low stacking-fault energy alloy. Phys Status Solidi 1983;75:525.
[66] Ezaz T, Sangid MD, Sehitoglu H. Energy barriers associated with slip-twin interactions. Philos Mag A, submitted for publication.
[67] Remy L. Twin–slip interaction in FCC crystals. Acta Metall 1977;25:711.
[68] Christian JW, Mahajan S. Deformation twinning. Prog Mater Sci 1995;39:1.
[69] Murr LE. Strain-induced dislocation emission from grain boundaries in stainless steel. Mater Sci Eng 1981;51:71.
[70] Valiev RZ, Gertsman VY, Kaibyshev OA. Grain boundary structure and properties under external influences. Phys Status Solidi A 1986;97:11.
[71] Deng C, Sansoz F. Fundamental differences in the plasticity of periodically twinned nanowires in Au, Ag, Al, Cu, Pb and Ni. Acta Mater 2009;57:6090.
[72] Deng C, Sansoz F. Effects of twin and surface facet on strain-rate sensitivity of gold nanowires at different temperatures. Phys Rev B Condens Matter Mater Phys 2010;81:155430.